# Self-organized network of phase oscillators coupled by activity-dependent interactions

Takaaki Aoki[1,*] and Toshio Aoyagi[2,3]
[1]*Faculty of Education, Kagawa University, Takamatsu 760-8521, Japan*
[2]*Graduate School of Informatics, Kyoto University, Kyoto 606-8501, Japan*
[3]*CREST, Japan Science and Technology Agency, Kawaguchi, Saitama 332-0012, Japan*
(Received 29 July 2011; published 14 December 2011)

We investigate a network of coupled phase oscillators whose interactions evolve dynamically depending on the relative phases between the oscillators. We found that this coevolving dynamical system robustly yields three basic states of collective behavior with their self-organized interactions. The first is the two-cluster state, in which the oscillators are organized into two synchronized groups. The second is the coherent state, in which the oscillators are arranged sequentially in time. The third is the chaotic state, in which the relative phases between oscillators and their coupling weights are chaotically shuffled. Furthermore, we demonstrate that self-assembled multiclusters can be designed by controlling the weight dynamics. Note that the phase patterns of the oscillators and the weighted network of interactions between them are simultaneously organized through this coevolving dynamics. We expect that these results will provide new insight into self-assembly mechanisms by which the collective behavior of a rhythmic system emerges as a result of the dynamics of adaptive interactions.

DOI: 10.1103/PhysRevE.84.066109 PACS number(s): 05.65.+b, 05.45.Xt, 89.75.Fb

## I. INTRODUCTION

Interaction is a key concept in statistical physics, and it essentially determines the emergent collective behavior of coupled dynamical systems. In many real-world systems, the interactions have large-scale, heterogeneous, and complex structures, and thus are suitable to be represented by the term "network." For example, many biological and social systems consist of a number of active elements that are structured in a complex network to be functional as a whole system. Recently, researchers have intensively investigated the statistical properties of real-world networks and revealed that the networks are not random but rather structured statistically [1–3]. However, little is known about the origin of these elaborate structures of networks. For example, how are the interactions of a network constructed to be functional as a whole system? We wish to elucidate the mechanism that allows the organized structures of networks to emerge as a natural process of their systems.

We hypothesize that the network structure of interactions in a system is organized depending on the activity of the system, rather than being completely predetermined. The networks in real-world systems are not static, but change over time. They adaptively reorganize in response to the activity of the systems. For example, recent neurophysiological experiments revealed that the change in synaptic connections depends on the relative timings between neuronal activities [4–6]. It is believed that this synaptic plasticity allows the real neuronal network to acquire a high capability of flexible brain functions. A chemical system of autocatalytic reactions is another example, in which the reaction rates of chemical interactions change dynamically depending on the reaction products of the system itself [7,8]. Many biological and social networks show similar activity-dependent plasticity related to functions of their systems [9–11].

Biological and social systems usually have no explicit system administrator who manages the interactions in the system, so the idea of self-organization of the network structure appears to be reasonable. However, the actual process of self-organization is still poorly understood. To examine the process, in this study we consider a dynamical system coupled by activity-dependent interactions and explore how the interactions are organized as a result of the asymptotic behavior of the dynamical system.

We studied a network of phase oscillators coupled by activity-dependent interactions, which was introduced in our previous paper [12]. In the model, together with the dynamics of the coupled oscillators, the strengths of the interactions evolve simultaneously depending on the relative timing between the oscillators, like the observed neural plasticity [4–6] (Sec. II). Through these coevolving dynamics, the relative phases of the oscillators and their interactions are coordinated as a result of the behavior of the dynamical system. In Sec. III, we describe asymptotic behaviors of the coevolving dynamical system and show that this system exhibits three distinct types of asymptotic behaviors: a two-cluster state, a coherent state, and a chaotic state. We discuss the robust emergence of these three states under various conditions in Sec. IV. Finally, we demonstrate that self-organized multiclusters can be realized by designing the dynamics of the coupling weights (Sec. V). Section VI summarizes our conclusions.

## II. A PHASE OSCILLATOR MODEL COUPLED BY ACTIVITY-DEPENDENT INTERACTIONS

We first consider the following equation of a coupled dynamical system:

$$\frac{d\mathbf{x}_i}{dt} = \mathbf{F}(\mathbf{x}_i) + \sum_j \mathbf{f}_{ij}(\mathbf{x}_i, \mathbf{x}_j),$$

where $\mathbf{x}_i$ denotes the state of the node $i$ of the network. The first term describes the intrinsic dynamics at the nodes, and the second term is the coupling term with the other nodes. In this study, we consider a limit-cycle oscillator as the intrinsic dynamics $\mathbf{F}$ for the following reasons: limit-cycle oscillation is widely observed in real dissipative systems, and coupled limit-cycle systems often generate a rich variety of collective

*aoki@ed.kagawa-u.ac.jp

 

behavior. Furthermore, limit-cycle oscillation is structurally stable, and it can be described by a simple model of a phase oscillator that is mathematically tractable. Therefore, it is reasonable to consider a limit-cycle oscillator as the intrinsic dynamics at the nodes. Using a standard reduction technique [13–15], the coupled limit-cycle system is described by the following equation:

$$\frac{d\phi_i}{dt} = \omega_i + \frac{1}{N}\sum_{j}^{N} k_{ij}\Gamma(\phi_i - \phi_j), \tag{1}$$

where $\phi_i$ denotes the phase of the limit-cycle oscillation at the $i$th node of the network ($i = 1, \ldots, N$), $\omega_i$ is its natural frequency, and $k_{ij}$ denotes the coupling weight of the connection from the $j$th to the $i$th oscillator. The coupling function $\Gamma(\phi)$ here is assumed to take the simple form $\Gamma(\phi) = -\sin(\phi + \alpha)$, because this first Fourier term is often dominant in many biological and chemical oscillators. Under suitable conditions, the parameter $\alpha$ can be regarded as the phase difference induced by a short transmission delay of the coupling [16]. For example, the parameter $\alpha$ could represent an axonal transmission delay in the synaptic connection of nerve systems or a delay in the reaction path in biochemical systems.

Next, we introduce the dynamics of the coupling weights $k_{ij}$ due to the activity-dependent plasticity of the weights. We assume that the plasticity depends on pure local information over a connection, not on nonlocal information over a network, such as the total number of links across a node and a global order parameter over the network. In other words, the weight dynamics only depends on the phases of the end-point nodes. Due to the translational symmetry of $\phi_i$, the dependency on the absolute values of the phases is neglected. Consequently, we denote the dynamics of the coupling weights $k_{ij}$ as follows:

$$\frac{dk_{ij}}{dt} = \epsilon\Lambda(\phi_i - \phi_j), \quad |k_{ij}| \leqslant 1. \tag{2}$$

In this equation, the plasticity of the network is governed by a function $\Lambda(\phi)$, which determines how the coupling weight depends on the relative timing of the oscillators. Thus, we call it a plasticity function. The time scale of this dynamics, represented by $\epsilon^{-1}$, is much longer than the time scale of the dynamics of the oscillators, i.e., $\epsilon \ll 1$, because the evolution of the connections is usually slower than that of the oscillators in real-world systems. The bounded condition $|k_{ij}| \leqslant 1$ implies that if $k_{ij}$ has a value outside the interval $[-1,1]$, it is immediately set to the appropriate bounded value ($-1$ or 1). This rule is reasonable because the weight cannot grow indefinitely. An alternative bounded condition can be implemented by adding a nonlinear term,

$$\frac{dk_{ij}}{dt} = \epsilon\left[\Lambda(\phi_i - \phi_j) - k_{ij}^{2\mu+1}\right],$$

where $\mu$ is an integer ($\mu \geqslant 0$). We numerically confirmed that for large $\mu$, this alternative implementation method gives qualitatively the same results.

In general, the plasticity function $\Lambda(\phi)$ is a $2\pi$-periodic function. Taking only the lowest-order Fourier mode into account for simplicity, we obtain the form $\Lambda(\phi) = -\sin(\phi + \beta)$. Under this condition, the characteristic of plasticity can be controlled by a single parameter $\beta$, as illustrated in Fig. 1. If $\beta \sim -\frac{\pi}{2}$, then the function $\Lambda(\phi)$ is similar to $\cos(\phi)$. In this case, for a pair of oscillators with similar phases, $\Lambda(\phi)$ gives a positive value, so the weight between them will be strengthened according to Eq. (2). In contrast, the weights between the oscillators of the different phases will be weakened. This characteristic of the plasticity is qualitatively similar to that of the Hebbian learning rule used in neuroscience [17]. We refer to this characteristic of plasticity as a Hebbian-like rule. If $\beta \sim 0$, then $\Lambda(\phi) \sim -\sin(\phi)$. The sign of the function is sensitive to the temporal order of the oscillators. When oscillator $i$ precedes oscillator $j$, the coupling weight from oscillator $i$ to $j$ is strengthened and the opposite weight is weakened. Therefore, it will encode a causal relation of activity of the oscillators into weights. This kind of plasticity has been observed in the cortex of the brain as a typical manner of spike-timing-dependent plasticity (STDP) [4–6]. We refer to this type of plasticity as a causal rule.[1] If $\beta \sim \frac{\pi}{2}$, then $\Lambda(\phi) \sim -\cos(\phi)$, which has the opposite effect of the Hebbian-like rule. We refer to this as an anti-Hebbian-like rule. Although we have explained three typical characteristics of plasticity, we never intended to restrict the plasticity rules. In this proposed model, the characteristic of plasticity is continuously changed by varying the parameter $\beta$, which enables us to investigate the coevolving dynamics in a systematic manner.

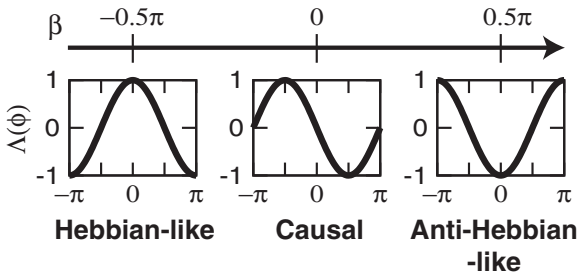


FIG. 1. The evolution of weights is determined by the plasticity function $\Lambda(\phi)$ parametrized by $\beta$. The characteristic of the plasticity changes continuously depending on the parameter $\beta$.

Taken together with the coupled dynamics of oscillators and the activity-dependent plasticity of the weights, the model proposed here is given by

$$\begin{aligned}\frac{d\phi_i}{dt} &= 1 - \frac{1}{N}\sum_{j} k_{ij}\sin(\phi_i - \phi_j + \alpha),\\ \frac{dk_{ij}}{dt} &= -\epsilon\sin(\phi_i - \phi_j + \beta), \quad |k_{ij}| \leqslant 1,\end{aligned} \tag{3}$$

where the natural frequencies are assumed to be identical, and we choose $\omega_i = 1$, without a loss of generality. We will discuss a case of various natural frequencies in Sec. IV A.

[1] This causal synaptic learning rule was referred to as a spike-timing-dependent plasticity (STDP) rule in our previous paper [12], because this rule is similar to the STDP seen in the cortex [4]. The STDP rules, however, vary depending on the area of the brain and species, and some of them are not causal [6]. Hence, we do not refer it as a STDP rule in this paper.

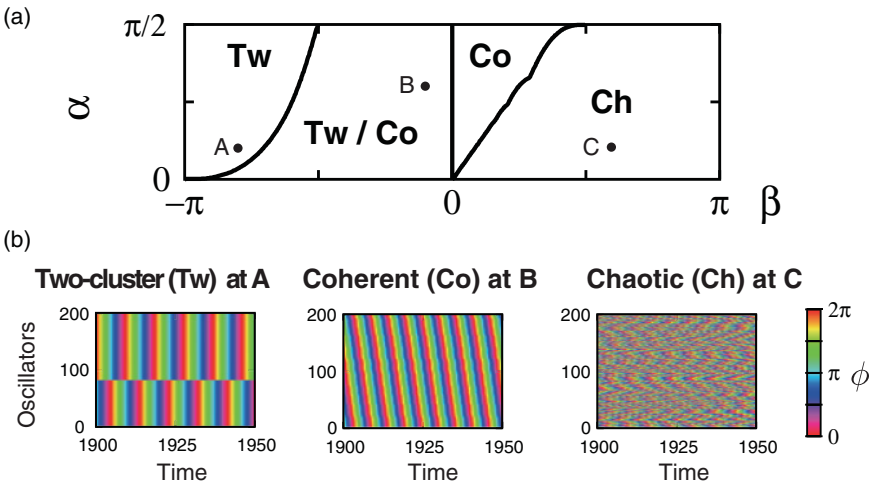


FIG. 2. (Color) (a) Phase diagram of the asymptotic states. (b) Phase patterns of the states. The graphs depict time developments of $\phi_i(t)$ using a color gradient ($t = 1900$–$2000$). The index $i$ of oscillators is arranged in order of increasing phase $\phi_i$ at a previous time ($t = 1000$). The number of oscillators $N = 200$. $\epsilon = 0.005$.

In the following numerical simulations, we investigate the asymptotic state of this dynamical system, given a random initial state, where the phases $\phi_i$ are chosen from a uniform distribution in $[0,2\pi)$ and the weights are chosen from a uniform distribution in $[-1,1]$. This system is characterized mainly by the two parameters $\alpha$ and $\beta$.[2] Hence, in later sections, we investigate the dependence of the asymptotic state of this model on these parameters.

## III. EMERGENCE OF THREE TYPICAL ASYMPTOTIC STATES FROM THE COEVOLVING DYNAMICS

In this section, we show that the proposed model exhibits three distinct asymptotic states that are structurally stable against perturbations. There are two distinct types of ordered states (two-cluster and coherent) and one disordered state (chaotic). Figure 2 shows a phase diagram of these states and their typical phase patterns of the coupled oscillators. In the following subsections, we will explain the properties of each of these states.

### A. Two-cluster state with synchronized oscillator groups

First, we explain the two-cluster state, in which the oscillators are organized into two clusters, as shown in Fig. 2(b). Figure 3(a) shows the properties of this state. The left graph displays the time development of the order parameters ($R_m = |\frac{1}{N}\sum_j e^{im\phi_j}|$, with $m = 1,2$), and a normalized rate of change of the weights averaged over all connections given by

$$\Delta K(t) = \frac{1}{N(N-1)} \sum_{i \neq j} \frac{|k_{ij}(t) - k_{ij}(t-\Delta)|}{\Delta},$$

where a sampling interval $\Delta \sim \frac{2\pi}{\omega} \ll \frac{1}{\epsilon}$. In this figure, the second order parameter $R_2$ converges to 1 and $R_1$ is kept to almost zero. This implies that the oscillators are organized into two synchronized groups with an antiphase relationship. The formation of the two groups is also confirmed in the middle graph in Fig. 3(a), which depicts the phase distribution after the transient period. We can see two significant peaks corresponding to the synchronized clusters in the phase distribution. Furthermore, the rate $\Delta K(t)$ converges to zero, which indicates that the weights become frozen. The right graph displays the weight matrix $k_{ij}(t)$ in the frozen state, in which the indices $i, j$ are arranged in the order of increasing phase $\phi_i(t)$ at the same time. From this graph, we can see that the reciprocal connections within the same cluster are in the state $k_{ij} = k_{ji} = 1$, whereas those between different clusters are in the state $k_{ij} = k_{ji} = -1$.

The formation of the two clusters is intuitively understood by the Hebbian-like characteristic of the plasticity function $\Lambda(\phi)$. In the region $\beta \in (-\pi,0)$, the function $\Lambda(\phi)$ induces the increase (decrease) of the weight $k_{ij}$ between in-phase (antiphase) oscillators. The increase (decrease) of the weight enhances the in-phase (antiphase) relationship of the oscillators. This is a kind of positive feedback of synchronization. In other words, the evolution of the weights follows a like-and-like (different-and-different) rule. Due to this characteristic of plasticity, a two-oscillator system in which a pair of oscillators is coupled reciprocally has two stable solutions in the region $\beta \in (-\pi,0)$ (see Appendix A). One is an in-phase solution, $k_{12} = k_{21} = 1, \Delta\phi = 0$, and the other is an antiphase solution, $k_{12} = k_{21} = -1, \Delta\phi = \pi$. For the $N$-oscillators system, any pair of oscillators satisfies either of these solutions in the two-cluster state. Therefore, the formation of the two-cluster state can be intuitively explained as follows: the like-and-like rule induces the formation of synchronized groups and the different-and-different rule separates the two groups into an antiphase relationship.

The ratio of the populations between the two clusters generally depends on the initial condition. In the graph, the size of the two clusters is almost equal since the initial phases were chosen uniformly from the range $[0,2\pi)$. If the initial phases are selected from a limited range, then the populations of the clusters are quite different. For example, if all oscillators almost synchronize at the initial time, then a single synchronized cluster emerges, which means that the ratio of populations between two clusters is 1:0. Thus, the formation of a single cluster is a specified case of the

[2]Note that this system is invariant under the translation $(\alpha,\beta,\phi_i) \to (-\alpha,\beta+\pi,-\phi_i)$ and $(\alpha,\beta,\phi_i) \to (\alpha+\pi,\beta+\pi,\phi_i)$. Due to this symmetry, it is sufficient to check the region $\alpha \in [0,\pi/2)$ and $\beta \in [-\pi,\pi)$.

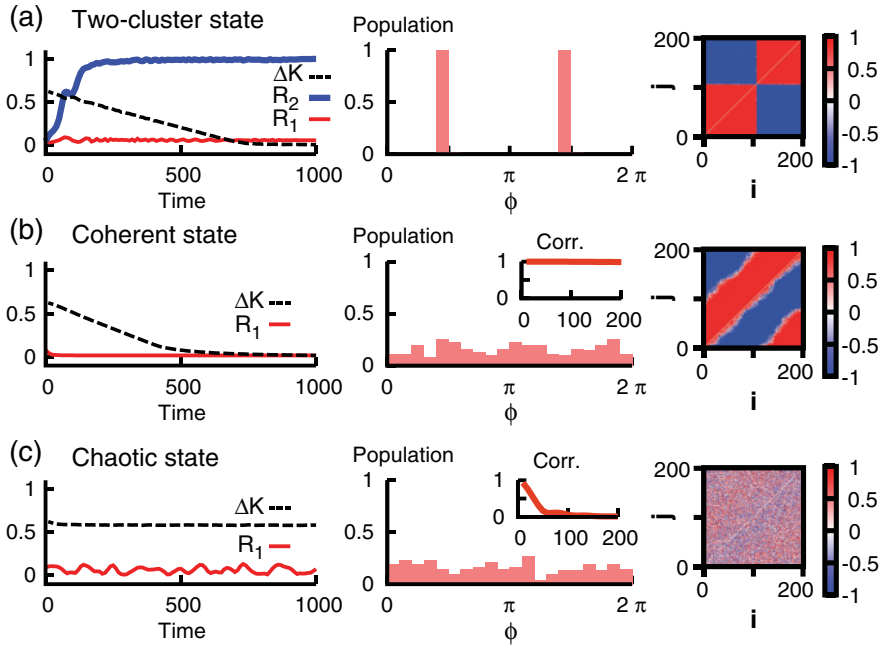


FIG. 3. (Color) Properties of the three asymptotic states. (Left) Order parameters $R_1, R_2$ and a normalized rate of change of the weights $\Delta K$. (Middle) Population of phases and autocorrelations of the relative phase relation. (Right) Weight matrix $k_{ij}$, in which the indices $i, j$ are arranged in the order of increasing phase. Parameter values are the same as in Fig. 2(b).

two-cluster state, and the initial condition determines whether two clusters or a single cluster emerges [18].

### B. Coherent state with a fixed phase relationship

The other ordered state is the coherent state, in which the oscillators are arranged in a sequence maintaining a fixed phase relation. This state has different properties from the two-cluster state, as shown in Fig. 3(b). The distribution of phases (the middle graph) is almost uniform and has no significant peak. The rate of change of weights $\Delta K$, however, converges to zero, which implies that the system settles into a steady state. To reveal the property of this steady state, we measured the autocorrelation function $C(\tau) = \langle |\frac{1}{N}\sum_j e^{i\phi_j(t)} e^{-i\phi_j(t-\tau)}| \rangle$, shown in the inset of the middle graph. From the graph, we can see that the autocorrelation does not decay and remains equal to unity. This means that relative phase relations among the oscillators are maintained in this steady state, that is, the oscillators are arranged in a sequence. Therefore, we refer to it as a coherent state.

The emergence of the coherent state is intuitively explained by the characteristic of the plasticity function $\Lambda(\phi)$. Around $\beta \sim 0$, $\Lambda(\phi) \sim -\sin(\phi)$, which encodes the causal relation of activity of the oscillators, because the sign of $\Lambda(\phi)$ depends on the temporal order of the oscillators. According to this causal rule of plasticity, a type of feed-forwarding network is organized, as shown in the right graph of Fig. 3(b). If oscillator $i$ precedes oscillator $j$ in the sequence, then the connection from $i$ to $j$ converges to the positive weight, $k_{ji} = 1$, and the opposite connection from $j$ to $i$ becomes the negative weight, $k_{ij} = -1$. More precisely, the weights satisfy the condition $k_{ij} = \mathrm{sgn}\,[-\sin(\phi_i - \phi_j + \beta)]$. These feed-forwarding connections maintain the temporal order of oscillators.

#### 1. Linear stability

Next, we analyze the linear stability of the coherent state against perturbations of the phases. In the limit $\epsilon \to 0$, the time scale of the weight dynamics, represented by $\epsilon^{-1}$, is slower than that of the coupled oscillators, and we only consider the stability of the phase pattern $\phi_i^*$ with the fixed weights, $k_{ij}^* = \mathrm{sgn}\,[-\sin(\phi_i^* - \phi_j^* + \beta)]$. If the phase pattern $\phi_i^*$ is stable, then the weights are also kept at the fixed values.

The eigenvalues of the coherent state are derived as

$$\mathrm{Re}\lambda_k = \begin{cases} -\frac{2}{\pi}\sin(\alpha-\beta) & (k \text{ is odd}), \\ -\frac{2}{\pi}\sin(\alpha-\beta) - \frac{2}{\pi(k^2-1)}[\cos k\beta \sin(\alpha-\beta) + k \sin k\beta \cos(\alpha-\beta)] & (k \text{ is even}), \end{cases}$$

where $k$ is the wave number of the deviation from the coherent state (see Appendix B).

The first eigenvalue, $\lambda_0 = 0$, corresponds to the uniform shift of the phases. Therefore, the stable region of the coherent state is determined by

$$\max_{k \geqslant 1} \mathrm{Re}\lambda_k < 0.$$

The phase diagram in Fig. 2(a) shows the stable region of the coherent state in the $(\alpha, \beta)$ plane. Similarly, the stable region of the two-cluster state is obtained (see Appendix B).

In order to examine how the coherent state is destabilized, we depict the boundaries between the coherent state and other states in Fig. 4. At the boundary between the coherent and the two-cluster states, the eigenvalue $\lambda_2$ becomes positive [Fig. 4(a)]. This boundary is expressed in the explicit

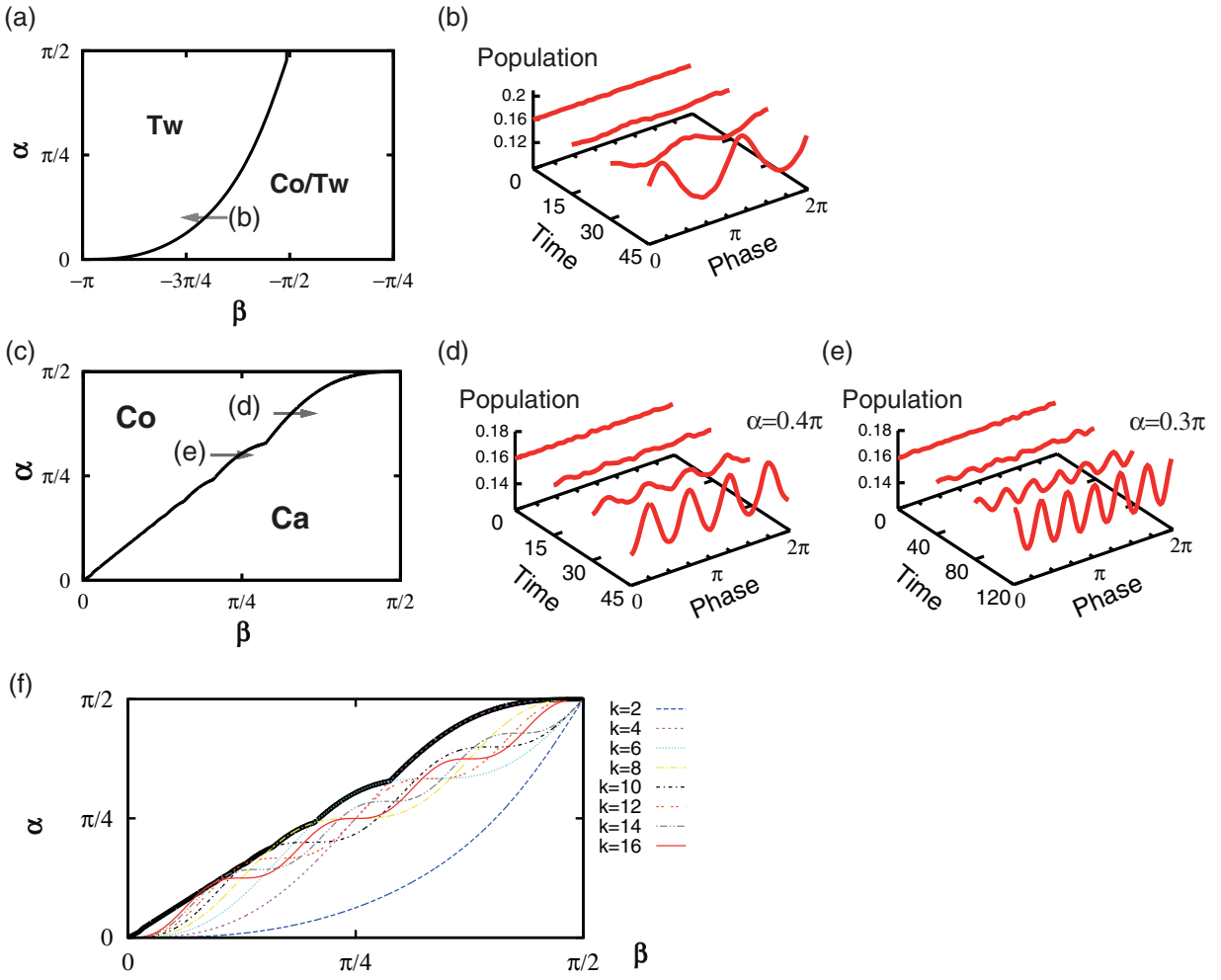


FIG. 4. (Color online) (a) The boundary between the coherent state and the two-cluster state. (b) The graph shows the time development of the phase population after the parameter $\beta$ is suddenly changed across the boundary as indicated by the arrow in Fig. 4(a). (c) The boundary between the coherent state and the chaotic state. (d,e) The graphs are the same as in (b). (d) The lines for wave number $k$ on which the eigenvalue $\lambda_k = 0$ ($k = 4, \ldots, 16$). The thick black line indicates the boundary where one of the eigenvalues becomes positive ($k \geqslant 1$).

form

$$\lambda_2 = 0 \Leftrightarrow \alpha = \sin^{-1}\left(\sqrt{\frac{8(\sin\beta)^6}{23 + 12\cos 2\beta - 3\cos 4\beta}}\right).$$

Figure 4(b) shows the time development of the phase population after destabilization of the coherent state induced by a sudden change in the value of $\beta$ as indicated by an arrow in Fig. 4(a). This graph shows that when the uniform phase distribution in the coherent state is disturbed, a deviation with the wave number $k = 2$ begins to develop, and finally the two clusters appear. Next, we examine the boundary of the chaotic states [Fig. 4(c)]. Figure 4(f) shows several lines of $\lambda_k = 0$. The coherent state becomes unstable when one of the eigenvalues $\lambda_k$ is positive. It depends on the parameter $\alpha$ whether the wave number $k$ becomes positive at first. We present two examples in Figs. 4(d) and 4(e). At $\alpha = 0.4\pi$ ($0.3\pi$), the eigenvalue $\lambda_4$ ($\lambda_6$) first becomes positive. We can see that the corresponding wave arises in the phase population as the time elapses. As a result, the boundary between the coherent and the chaotic states consists of pieces of the lines of $\lambda_k = 0$ ($k = 4,6,8, \ldots, \infty$). This result supports the emergence of the chaotic state.

### 2. *Bistability*

The phase diagram shown in Fig. 2(a) indicates that there is a bistable region between the two-cluster and the coherent states. The initial condition determines which of these states is realized. In an unbiased initial condition, where the phases $\phi_i$ are chosen from a uniform distribution in $[0,2\pi)$ and the weights are chosen from a uniform distribution in $[-1,1]$, the system appears to be in the coherent state for $\alpha > -\beta$ and in the two-cluster state elsewhere. It should be noted that once the system is settled in either of these states, a transition between the states never occurs, because these asymptotic states are stable.

Moreover, we can consider a combination of coherent and two-cluster states, in which several synchronized groups are arranged in a sequence. Considering $M$ groups of synchronized oscillators, $\phi_i^m = \phi^m$ ($m = 1,2, \ldots, M$), any pairs of oscillators within the groups satisfy the in-phase solution, $k_{ij} = k_{ji} = 1, \Delta\phi = 0$, as in the two-cluster state. Thus, each

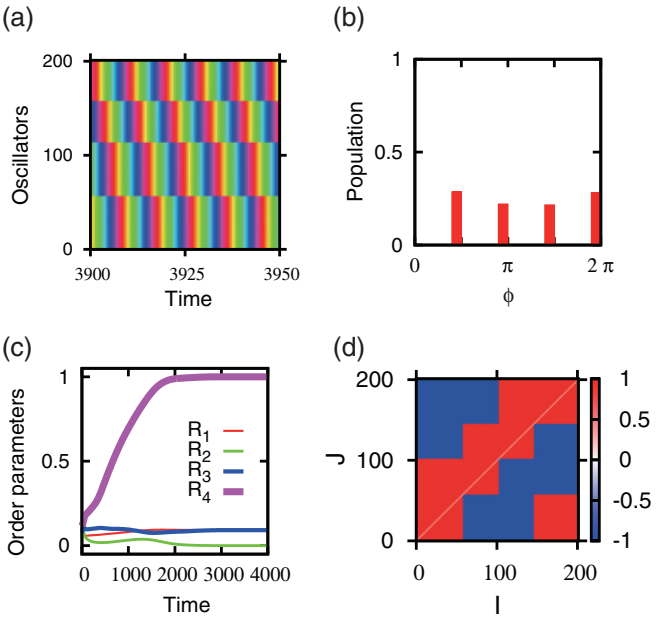


FIG. 5. (Color) Emergence of four clusters by a combination of the two-cluster and coherent states. $\alpha = 0.4\pi$, $\beta = -0.3\pi$. (a) Time developments of $\phi_i(t)$. (b) Phase distribution at $t = 4000$. (c) Time developments of order parameters, $R_1, R_2, R_3, R_4$. (d) Weight matrix $k_{ij}$ at $t = 4000$.

group can be regarded as a single bundled oscillator and we obtain the same equation for the bundled oscillators $\phi^m$ as in Eq. (3), unless the coupling weights between the groups are bundled into the total value. Then, there is a solution to the coherent state for the equation of the bundled oscillators. This combination of both states looks like an $M$-cluster state. Actually, we present an example of a four-cluster state observed in the bistable region in Fig. 5. Note that the initial conditions generating this $M$-cluster state are somewhat rare and the perfect $M$ cluster is not usually observed from random initial conditions. Under random initial conditions, instead of the emergence of the perfect $M$-cluster state, we can observe several small-sized clusters in the coherent state, while most of oscillators are separated with distinct phases. In Fig. 3(b), the phase distribution is not completely flat, which indicates the existence of small-sized clusters.

### C. Emergence of the chaotic state by self-breaking of the time-scale separation in the coevolving dynamics

In the other parameter region, where both the two-cluster and the coherent states are unstable, the system exhibits chaotic behavior. As shown in Fig. 3(c), the rate of change of weights $\Delta K$ does not converge to zero and the autocorrelation $C(\tau)$ quickly decays to zero. The population of the phases, shown in the middle graph, has no particular peak. No distinct structure in the weight matrix $k_{ij}$ is observed. This indicates that the system does not settle into a fixed state. The weights and the relative phase relations continue to change in time through the coevolving dynamics.

To investigate the property of this disordered behavior, we consider the two-oscillator system (see Appendix A). This system is given by an equation of three variables $\Delta\phi, k_{12}, k_{21}$ as

$$\begin{aligned} \frac{d\Delta\phi}{dt} &= -k_{12}\sin(\Delta\phi+\alpha) + k_{21}\sin(-\Delta\phi+\alpha), \\ \frac{dk_{12}}{dt} &= -\epsilon\sin(\Delta\phi+\beta), \quad \frac{dk_{21}}{dt} = -\epsilon\sin(-\Delta\phi+\beta). \end{aligned} \tag{4}$$

In the limit $\epsilon \to 0$, using this adiabatic approximation, we obtain the reduced equation

$$\begin{aligned} \frac{dk_{12}}{dt} &= -\epsilon\sin[\Delta\phi^*(k_{12},k_{21}) + \beta], \\ \frac{dk_{21}}{dt} &= -\epsilon\sin[-\Delta\phi^*(k_{12},k_{21}) + \beta], \end{aligned} \tag{5}$$

where the dynamics are described only by the weights $k_{12}, k_{21}$. Figure 6(a) shows a phase portrait of the system described by Eq. (5) in the $(k_{12}, k_{21})$ plane. In the graph, there is a global attractor at $k_{12} = k_{21} = 0$. At this fixed point, however, the adiabatic approximation does not hold even in the limit $\epsilon \to 0$. As both weights approach zero, the convergence of the variable $\Delta\phi$ to the equilibrium $\Delta\phi^*$ slows down significantly, and eventually becomes of the same order as that for the dynamics of the weights. This implies that the time-scale separation between the dynamics of the relative phase and that of the weights breaks as a result of their own dynamics. Researchers have often discussed the time-scale separation between the network reformation and activity at the nodes, and expected that the breaking of the time-scale separation would bring a remarkable behavior in adaptive networks [19–21]. Our result provides an interesting example. The breaking of the time-scale separation is induced by its own dynamics. Furthermore, after the time-scale separation is broken, a chaotic behavior emerges. Figure 6(b) displays a typical trajectory of the system without the adiabatic approximation given in Eq. (4). In Figs. 6(b) and 6(c), we can see two vertices around $\Delta\phi = \pm\frac{\pi}{2}$ and a number of paths between these vertices. When a point of the state of this dynamical system sinks in either of the vertices, it slowly changes the weights around the center of the vertex, and then it suddenly jumps into the other vertex and repeats. We found that the largest Lyapunov exponent is positive, as shown in Fig. 6(d). Therefore, we refer to this state as a chaotic state. The $N$-oscillators system also has positive Lyapunov exponents. The number of positive Lyapunov exponents is proportional to the number of degrees of freedom of the dynamical system, $N^2$ [Fig. 6(e)].

The emergence of such a disordered state is intuitively explained by the anti-Hebbian-like characteristic of the plasticity function $\Lambda(\phi)$. In the chaotic state, $\Lambda(\phi)$ weakens the connections between the pair of synchronized oscillators, and eventually the oscillators become desynchronized. This means that the evolution of the weights destroys the structure of the connections that realize the current relations among oscillators. Therefore, the disordered state is intuitively understood by the following process: (i) The phase pattern causes the structure of the weighted network to change. (ii) The change undergone by the weights causes a new phase pattern to appear. (iii) The change of the phase pattern results in further modulation of the weights of the network. (iv) This process repeats. Note that in the actual process, the oscillators and the weights evolve simultaneously, not in a step-by-step manner.

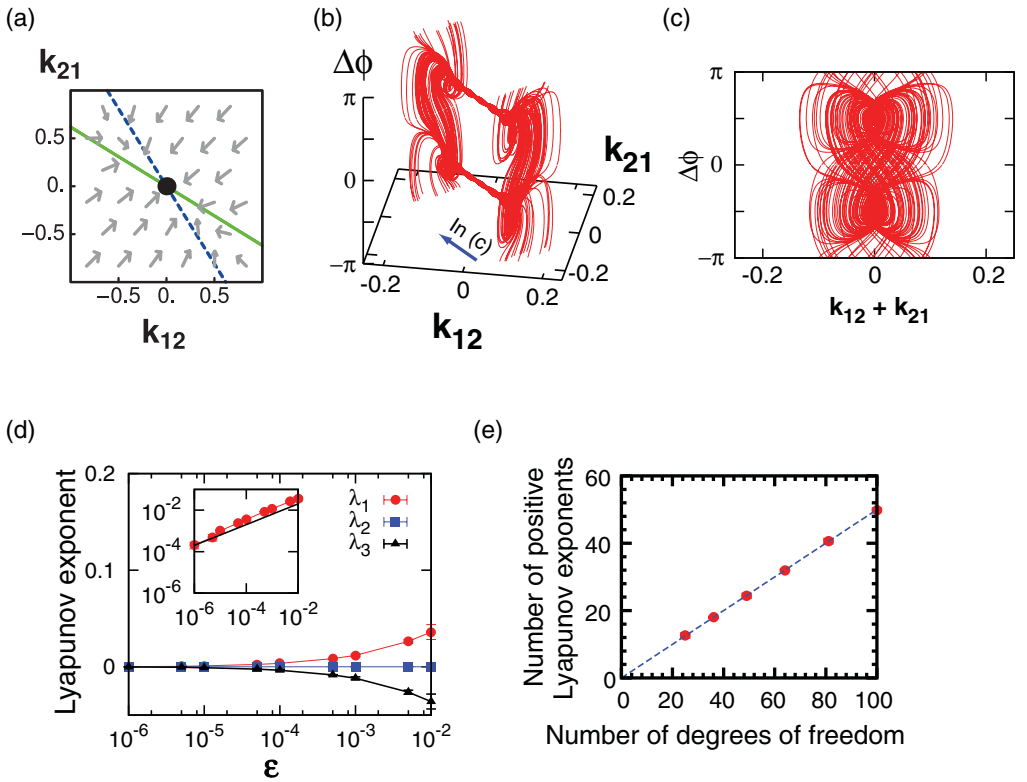


FIG. 6. (Color online) A chaotic state caused by the coevolving dynamics of weights and oscillators. (a) Phase portraits of the system in the $(k_{12},k_{21})$ plane obtained using an adiabatic approximation in the chaotic state. $\beta = 0.7\pi$ and $\alpha = 0.1\pi$. (b) A trajectory in the chaotic state of the two-oscillator system, with $\alpha = 0.05\pi$, $\beta = 0.65\pi$, and $\epsilon = 0.005$. (c) The same trajectory of (b) projected on the $(\Delta\phi,k_{12}+k_{21})$ plane. (d) Lyapunov exponents as functions of $\epsilon$. The inset displays a log-log plot, with a fitting curve satisfying $\lambda \propto \epsilon^{1/2}$. The parameters are the same as in (b). (e) The number of positive Lyapunov exponents as a function of the number of degrees of freedom of the system, $N^2$. $\beta = 0.7\pi$ and $\alpha = 0.2\pi$.

## IV. ROBUST EMERGENCE OF THE THREE TYPES OF ASYMPTOTIC STATES

Next, we discuss the robust emergence of the three states mentioned in the previous section.

### A. Effects of the variations in the frequencies of oscillators

In the previous sections, we assumed that all oscillators are identical. However, this is unnatural, because practical oscillators have differing frequencies. Here we consider whether the observed states still emerge with nonidentical oscillators even from random initial weights and phases. The frequency of the oscillator, $\omega_i$, is generated from a normal distribution with a deviation $\sigma_\omega$. The initial conditions for $k_{ij}$ and $\phi_i$ are chosen randomly from a uniform distribution on $[-1,1]$ and $[0,2\pi)$, respectively.

Figure 7 shows three measures as a function of $\beta$ for several $\sigma_\omega$: the second order parameter $\bar{R}_2$, the long-time correlation $\bar{C}$ $[= C(\tau^*), \tau^* = 200]$, and the rate of change of weights $\overline{\Delta K}$. These measures denoted by a diacritical mark $\bar{X}$ are evaluated by averaging over a long period after removing a transient period. Each data point in the figure is estimated from 40 trials with various initial conditions and various sets of natural frequencies of the oscillators. As mentioned in the previous sections, the second order parameter $\bar{R}_2$ converges to 1 in the two-cluster state. If $\bar{R}_2$ converges to 0, but the long-time correlation $\bar{C}$ is still 1, then the system is in the coherent state. When the rate of change of weights $\overline{\Delta K}$ does not converge to zero, the system is in the disordered (chaotic) state. In the figure, the profile of these measures indicates that the system converges to one of the three states depending on $\beta$, as in the case of identical oscillators. Hence, we can conclude that the three states are still observed with nonidentical oscillators. Moreover, we found that variation in the natural frequency increases the convergence time drastically. Figure 8 depicts the time development of the second order parameter $R_2$ when the two-cluster state appears. It reveals that the convergence to the two-cluster state becomes much slower as frequency variation, denoted by $\sigma_\omega$, increases. By rescaling the time and the weights, $\sigma_\omega$ is absorbed into $\epsilon$ $(=\frac{\epsilon}{\sigma_\omega^2})$. $\epsilon$ is the parameter of the changing rate of weights, so the increase of $\sigma_\omega$ slows the change of weights.

### B. Effects of perturbations in the plasticity function $\Lambda(\phi)$

In the model, the plasticity of the coupling weight is determined by the function $\Lambda(\phi)$ and we assume the form of the function as $\Lambda(\phi) = -\sin(\phi+\beta)$, taking only the lowest-order Fourier mode into account for simplicity. In this subsection, we consider small perturbations in the function $\Lambda(\phi)$ and evaluate the effect of the perturbations on the emergence of the asymptotic states.

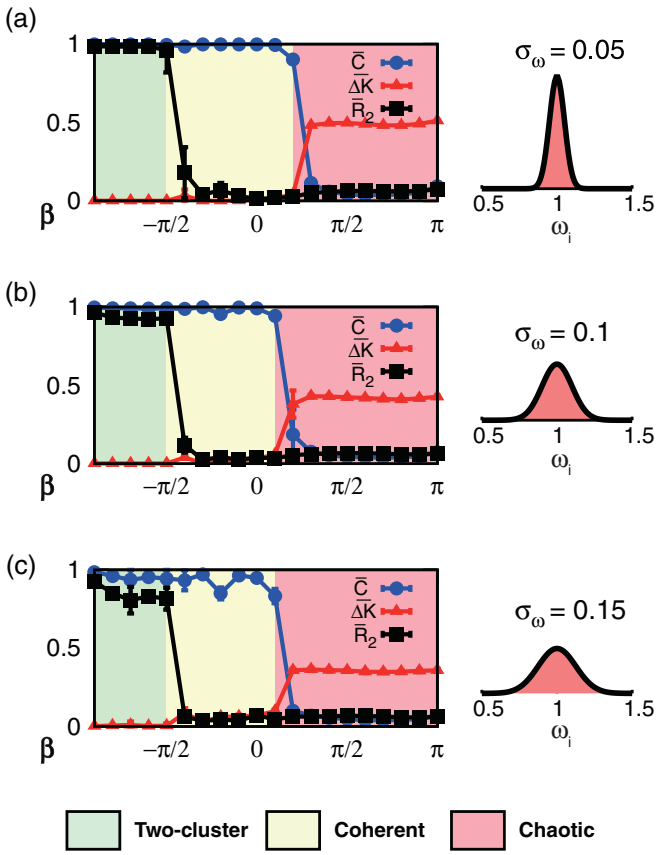


FIG. 7. (Color online) Emergence of the three states in the case of various natural frequencies of the oscillators, $\omega_i$. Three measures as a function of $\beta$ for several $\sigma_\omega$: the second order parameter $\bar{R}_2$, the correlation $\bar{C}$, and the rate of change of weights $\overline{\Delta K}$. The parameters are as follows: $\alpha = 0.3\pi$, $\epsilon = 0.005$. (a) $\sigma_\omega = 0.05$, (b) $\sigma_\omega = 0.1$, (c) $\sigma_\omega = 0.15$.

First, let us attempt to consider a biased function $\bar{\Lambda}(\phi)$ given by

$$\bar{\Lambda}(\phi) = \Lambda_0 - \sin(\phi + \beta).$$

The plasticity has a bias $\Lambda_0$ $[= \int_0^{2\pi} \bar{\Lambda}(\phi)d\phi]$ toward an increase or a decrease of the weight, which potentially causes the system behavior to change drastically. Varying the bias $\Lambda_0$, we examined whether the system converges to the three states from a random initial condition. Figure 9 shows the three measures, $\bar{R}_2, \bar{C}, \overline{\Delta K}$. The profiles of these measures

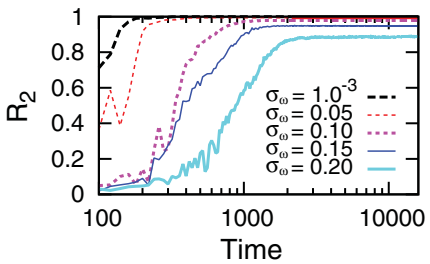


FIG. 8. (Color online) Time development of the second order parameter $R_2$ for several $\sigma_\omega$ in the two-cluster state. $\beta = -0.7\pi$, $\alpha = 0.1\pi$, $\epsilon = 0.01$.

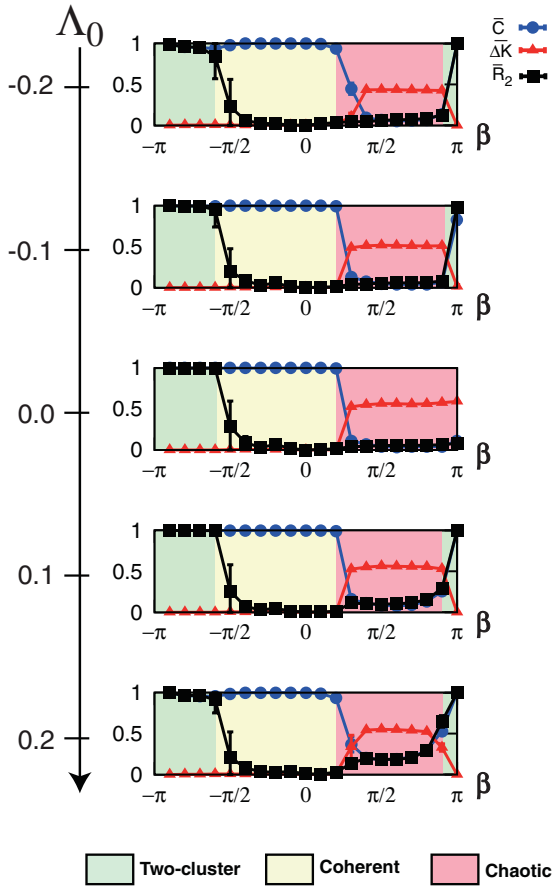


FIG. 9. (Color online) Emergence of the three states under a biased plasticity. The biased plasticity function $\bar{\Lambda}(\phi)$ is a perturbed function of the plasticity with a bias $\Lambda_0$ $[= \int_0^{2\pi} \bar{\Lambda}(\phi)d\phi]$ toward an increase or a decrease of the weights. Each graph shows three measures as a function of $\beta$ for several $\Lambda_0$: the second order parameter $\bar{R}_2$, the long-time correlation $\bar{C}$, and the rate of change of weights $\overline{\Delta K}$. $\alpha = 0.3\pi$ and $\epsilon = 0.005$. Each data point is estimated from 20 trials with various initial conditions.

indicate that the system still exhibits the three asymptotic states depending on $\beta$, even if the bias $\Lambda_0 \neq 0$. Note that the boundaries between the three states are slightly modulated by the bias $\Lambda_0$. Hence, under the biased plasticity, the system exhibits qualitatively the same behavior as with unbiased plasticity.

Next, we discuss the stability of the two-cluster and coherent states against a perturbation of the plasticity function. We consider a plasticity function containing small higher Fourier modes,

$$\tilde{\Lambda}(\phi) = -\sin(\phi + \beta) + \sum_{m=2}^{M} c_m \sin(m\phi + \beta_m),$$

where $\sum_{m=2}^{M} |c_m| \ll 1$. In both ordered states, the coupling weights take either of the limiting values, 1 or $-1$. These values remain unchanged unless the perturbation alters the sign of $\Lambda(\phi)$. This means that the stability of both states is guaranteed by the condition $|\sin(\Delta\phi + \beta)| > \sum |c_m|$. In the case of the two-cluster state, the relative phases among oscillators take only two values: $\Delta\phi = 0, \pi$, and the stability condition is

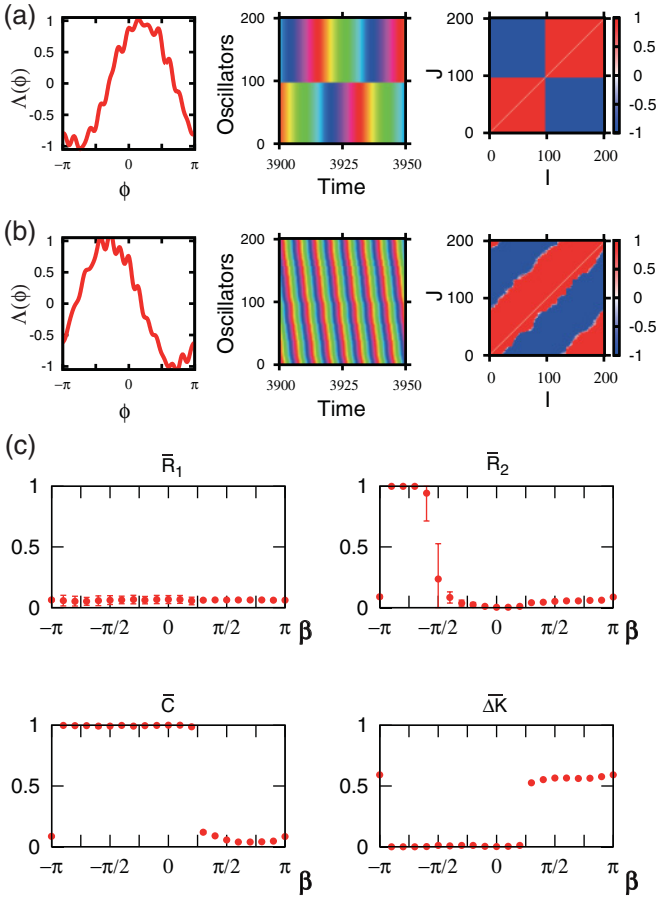


FIG. 10. (Color) Self-organization by a perturbed plasticity function $\tilde{\Lambda}(\phi)$, which contains small higher Fourier modes. (a) Example of the two-cluster state. (Left) A perturbed plasticity function. (Middle) Time development of phases $\phi_i(t)$. (Right) The coupling weights $k_{ij}$ organized by the coevolving dynamics. $\alpha = 0.3\pi$. $\beta = -0.7\pi$. (b) Example of the coherent state. $\alpha = 0.3\pi$. $\beta = -0.2\pi$. (c) Each graph shows three measures in a stationary state as a function of $\beta$: the order parameters $\bar{R}_1$ and $\bar{R}_2$, the correlation $\bar{C}$, and the rate of change of weights $\overline{\Delta K}$. $\alpha = 0.3\pi$ and $\epsilon = 0.005$. Each data point is evaluated by randomly perturbed functions $\tilde{\Lambda}(\phi)$.

to be checked only at these two values. Considering a small positive value $\delta$ ($\sim \sum |c_m|$), the stability condition holds in the range $\beta \in [\delta, \pi - \delta]$. This implies that the two-cluster state is structurally stable against this perturbation, although the boundary of the two-cluster state changes slightly. In the coherent state, the relative phases among oscillators are uniform in $[-\pi,\pi]$. Therefore, a few pairs of oscillators for which $|\sin(\Delta\phi + \beta)| \sim \delta$ do not meet the stability condition, and the coupling weights between them, can be affected by the perturbation, although most pairs of oscillators are unchanged. This means that a few coupling weights ($\sim\delta$) among the oscillators can be altered by the perturbation. This situation is similar to a failure of a network, in which a few connections of the network are not functioning. Next, we numerically confirmed the stability of the coherent state and summarized it in Fig. 10. The perturbation of $\Lambda(\phi)$ is randomly determined for each trial (50 trials for each $\beta$). The amplitudes of higher modes, $c_m$, are randomly selected from a uniform distribution, keeping a condition $\sum |c_m| = 0.1$. $\beta_m$ is chosen uniformly from $[-\pi,\pi]$. The maximum mode $M$ is set to be 15. Figure 10(c) depicts the measures as a function of $\beta$: the order parameters $\bar{R}_1, \bar{R}_2$, the long-time correlation $\bar{C}$, and the rate of change of weights $\overline{\Delta K}$. The profile of these measures indicates that the two-cluster and coherent states are stably organized by the perturbed plasticity functions. Actually, the graphs in Figs. 10(a) and 10(b) show examples of the two-cluster state and the coherent state, respectively. Hence, these ordered states are not affected by a small perturbation in the function $\Lambda(\phi)$.

### C. Coevolving dynamics on a scale-free network

We consider a topology of the connections in the coevolving dynamics. In the previous sections, we have assumed a case of the all-to-all connections for simplicity, in which each oscillator is coupled with the other oscillators. However, real-world networks have complex topological structures of their connections, such as scale-free, small-world, and modules [22–24]. The collective synchronization on the static complex networks has already been investigated extensively [25–32]. In the next stage, these topological structures should be involved in the coevolving dynamics both on and of a network.

In this section, we focus on the effect of network topology on the coevolving dynamics. Specifically, we examine whether the asymptotic states found in the all-to-all connections are still observed on a scale-free network. We assume here that the scale-free topology is given before the procedure of coevolving dynamics and is not changed through the coevolving dynamics. Then, the coevolving dynamics of oscillators and weights is given by

$$\frac{d\phi_i}{dt} = 1 - \frac{1}{N_i} \sum_{j\in\{\mathcal{N}_i\}} k_{ij} \sin(\phi_i - \phi_j + \alpha),$$

$$\frac{dk_{ij}}{dt} = -\epsilon \sin(\phi_i - \phi_j + \beta), \quad |k_{ij}| \leqslant 1,$$

where $\{\mathcal{N}_i\}$ is a set of nodes connecting to the $i$th node and $N_i$ is the number of nodes in the set. The topology of connections is generated by the Barabási-Albert (BA) model [23] for each trial, characterized by the following parameters: the number of additional nodes for each step $m = 5$, the number of initial nodes $m_0 = 10$, and the total number of nodes $N = 1000$. We numerically confirmed that these parameter values do not critically affect the following results. Figure 11(a) illustrates an example of the generated scale-free network. The mean number of connections in this network is significantly smaller than the all-to-all network. With the given parameter values, the number of connections is about $2mN$ ($=10^4$) for the scale-free network and $N^2$ ($=10^6$) for the all-to-all network. Despite this significant difference in the connections, we found that the system behavior of the scale-free network is qualitatively the same as that of the all-to-all one and the three asymptotic states still emerge, as shown in Figs. 11(b)–11(e). In the two-cluster and coherent states, no significant relationship is observed between the organized relative phases and the degree of the nodes in the scale-free network. Therefore, the topological difference between the scale-free and the all-to-all connections has no considerable effect on the emergence of the three asymptotic behaviors in this situation. This result is not surprising. It has been reported that the coupled dynamics

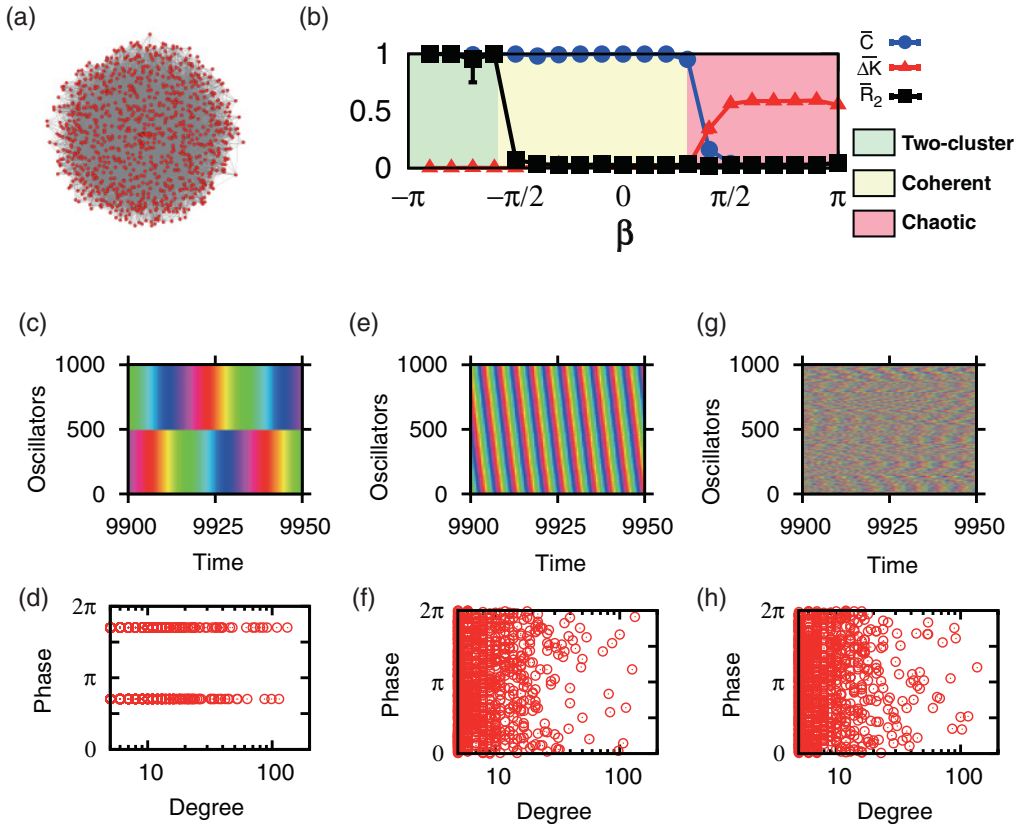


FIG. 11. (Color online) Coevolving dynamics of weights and oscillators on a scale-free network. (a) The topology is generated by the Barabási-Albert model for each trial. The number of additional links at each step $m = 5$, the number of initial nodes $m_0 = 10$, and the total number of nodes $N = 1000$. (b) Three measures as a function of $\beta$: the second order parameter $\bar{R}_2$, the long-time correlation $\bar{C}$, and the rate of change of weights $\overline{\Delta K}$. $\alpha = 0.3\pi$, $\epsilon = 0.005$. (c,d) Example of the two-cluster state. (Left) Time developments of $\phi_i(t)$. (Right) Relationship between the node degree and the phases. $\beta = -0.7\pi$, $\alpha = 0.3\pi$. (e,f) Example of the coherent state. $\beta = -0.1\pi$, $\alpha = 0.3\pi$. (g,h) Example of the chaotic state. $\beta = 0.7\pi$, $\alpha = 0.3\pi$.

on the scale-free network generated by the BA model is well described using the mean-field approximation, which is exact in the case of all-to-all coupling [26,33,34]. Our result supports this conjecture.

In this case, we assumed that the network topology is not modified by the coevolving dynamics in order to eliminate additional effects on the network topology and clarify the pure effects of the scale-free topology on the dynamics. However, the evolution of topology is closely related to the dynamics at the nodes in general. A series of studies of coevolving dynamics incorporating the evolution of topology, such as creation, deletion, and rewiring of links, are required to find novel concepts to capture the essential network topology related to the functional activity of network-based dynamical systems.

## V. DESIGNING MULTICLUSTER STATES

We have examined the three types of asymptotic behaviors of the coupled oscillator system described by Eq. (3). In this section, let us consider other types of behaviors of the coevolving dynamical system given by Eqs. (1) and (2), designing the plasticity function $\Lambda(\phi)$. We present a designed multicluster state that can be self-organized even from a random initial state.

As mentioned in the previous sections, the system exhibits the two-cluster state, in which the oscillators are organized into two synchronized groups. This result leads to a natural question of whether this system has another multicluster state, and, if so, how to control the number of clusters as desired. In the coupled oscillator system given by Eqs. (1) and (2), the asymptotic behavior of oscillators can be designed by choosing an appropriate plasticity function $\Lambda(\phi)$. Figure 12 displays such examples. Using the function $\Lambda(\phi) = \cos(2\phi - 0.1\pi)$, this system exhibits a three-cluster state even from random initial weights and phases. The function $\Lambda(\phi) = \cos(3\phi - 0.1\pi)$ generates a four-cluster state. We numerically found that the $m$-cluster state is observed for $\Lambda(\phi) \sim \cos[(m-1)\phi]$. Hence, this model exhibits a variety of behaviors depending on the form of the plasticity function $\Lambda(\phi)$, which will provide a simple framework for designing self-assembled collective behaviors in dynamical systems.

## VI. DISCUSSIONS

We have investigated a network of coupled phase oscillators, in which both the phases of oscillators and the coupling weights evolve simultaneously. Through this interplay of oscillators and coupling weights, the relative phases of the

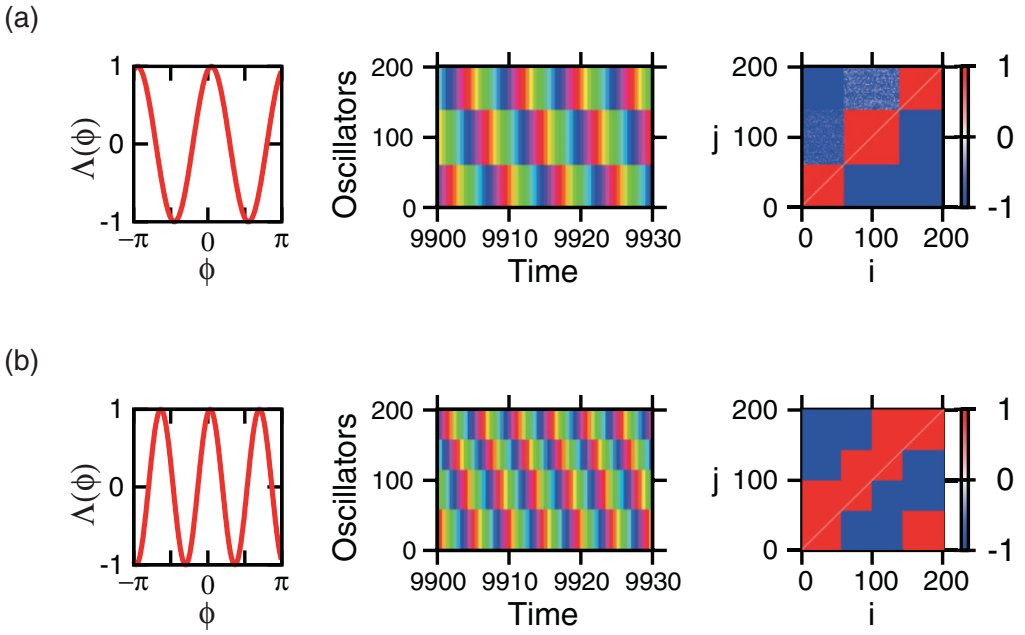


FIG. 12. (Color) A multicluster state designed by choosing an appropriate plasticity function $\Lambda(\phi)$. (a) Three-cluster state. (b) Four-cluster state. The left graph shows the plasticity function $\Lambda(\phi)$. The middle graph depicts the phases $\phi_i(t)$ in which the indexes $i$ of oscillators are arranged in order of increasing phase at a previous time, $t = 8000$. The right graph shows the weight matrix $k_{ij}$ at the stationary state. $\alpha = 0.1\pi$ and $\epsilon = 0.005$.

oscillators and their weights are coordinated as a result of the behavior of the dynamical system.

When the dynamics of the weights are governed by a sinusoidal function of relative phases, we found that this coevolving dynamical system robustly yields three distinct types of self-organized phase patterns of oscillators with structured weights: the two-cluster state, the coherent state, and the chaotic state. Furthermore, we demonstrated that self-assembled multiclusters can be designed by controlling the plasticity function.

A number of studies have revealed that coupled oscillator systems can exhibit a wide variety of spatiotemporal patterns, including several types of clustered, phase-locked, and turbulent states, even when the oscillators are coupled globally or diffusively with static coupling weights [35–42]. When compared with these phase patterns, our results emphasized that the phase patterns of the oscillators and the weighted network of interactions between them are simultaneously self-organized through the coevolving dynamics even if the initial coupling weights are randomly disordered. In other words, the coevolving dynamics generates the patterns of the phases as well as the weights.

The generated patterns in the asymptotic states have several different characteristics compared with the similar phase patterns observed in the the conventional coupled phase oscillators. It is known that globally coupled phase oscillators can generate two or more clusters if coupling function $\Gamma(\phi)$ has a second or higher Fourier mode, and the ratio of the populations among the organized clusters is related to the phase difference between the clusters in general [36–38]. In contrast, our model can exhibit the two-cluster state even when the coupling function $\Gamma(\phi)$ has only the first Fourier mode. The phase difference between the clusters is maintained at $\pi$; however, the ratio of the populations depends on the initial state, as mentioned in Sec. III A. Furthermore, in the two-cluster and coherent states, information regarding the phase relationship between the oscillators is stored in the coupling weights between them, because the coupling weights are related to the phase relationships through the coevolving dynamics.

The collective behavior of coupled oscillators with activity-dependent interaction has been studied recently under various conditions [21,43–51]. Furthermore, other types of dynamics on adaptive networks have been studied in several fields of science [52–58]. In addition, coupled dynamics on randomly time-varying networks have been reported [59–63]. Therefore, it is necessary to summarize the various behaviors of a coevolving dynamical system across their fields and draw a clear perspective. We believe that our model will provide a simple framework to understand the nature of coevolving dynamical systems, which will help us to elucidate the mechanism by which the organized structures of real-world networks emerge as a natural process of their dynamical systems.

## ACKNOWLEDGMENTS

This work was supported by KAKENHI (19GS0208, 21120002, 23115511).

## APPENDIX A: TWO-OSCILLATOR SYSTEM

In this appendix, we consider a two-oscillator system, in which a pair of oscillators is coupled by reciprocal connections.

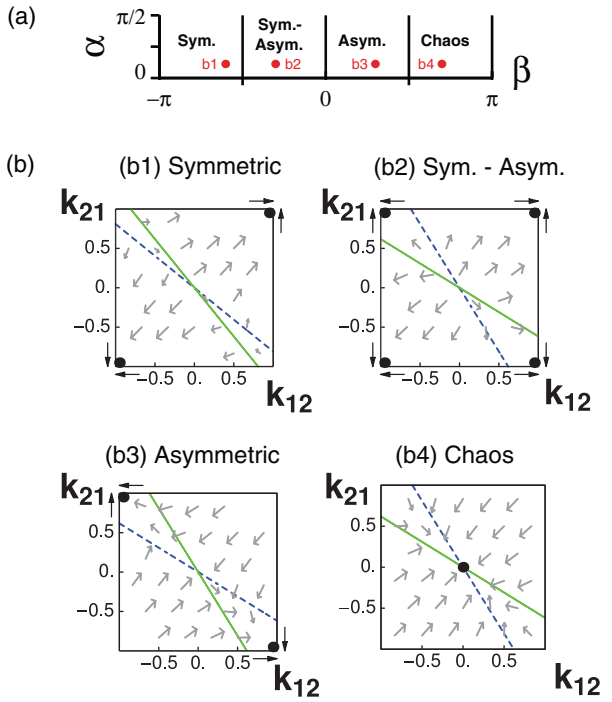


FIG. 13. (Color online) (a) Phase diagram of a two-oscillator system. The asymptotic states can be classified into three types: symmetric, asymmetric, and chaotic. In the bistable region, both the symmetric and asymmetric states are stable. (b) Phase portraits of the system in the $(k_{12},k_{21})$ plane were obtained using an adiabatic approximation in Eq. (A2). The parameters $(\alpha,\beta)$ of these phase portraits correspond to the red points (b1–b4) in graph (a). The blue and green lines represent the nullclines for $k_{12}$ and $k_{21}$, respectively. The black circles indicate stable fixed points. It is noted that the weight $k_{ij}$ is bounded in a region $[-1,1]$.

In this case, the dynamics can be written in terms of three variables, $\Delta\phi$ $(\equiv\phi_1-\phi_2)$, $k_{12}$, and $k_{21}$, as

$$\begin{aligned}\frac{d\Delta\phi}{dt}&=-k_{12}\sin(\Delta\phi+\alpha)+k_{21}\sin(-\Delta\phi+\alpha),\\ \frac{dk_{12}}{dt}&=-\epsilon\sin(\Delta\phi+\beta),\quad \frac{dk_{21}}{dt}=-\epsilon\sin(-\Delta\phi+\beta).\end{aligned}\tag{A1}$$

The condition $\epsilon\ll 1$ implies that $\Delta\phi$ is the fast variable and $k_{12}$ and $k_{21}$ are slow variables. Therefore, $\Delta\phi$ quickly relaxes to the equilibrium value, $\Delta\phi^*$. The value $\Delta\phi^*$ is given by the condition $\tan(\Delta\phi^*)=-\frac{k_{12}-k_{21}}{k_{12}+k_{21}}\tan\alpha$, obtained from $\frac{d\Delta\phi}{dt}=0$. We can thus eliminate the variable $\Delta\phi$ in Eq. (A1). This equation thereby reduces to

$$\begin{aligned}\frac{dk_{12}}{dt}&=-\epsilon\sin[\Delta\phi^*(k_{12},k_{21})+\beta],\\ \frac{dk_{21}}{dt}&=-\epsilon\sin[-\Delta\phi^*(k_{12},k_{21})+\beta].\end{aligned}\tag{A2}$$

In addition to the fixed point of this dynamical system satisfying $\frac{dk_{12}}{dt}=\frac{dk_{21}}{dt}=0$, there is another type of steady state, in which the weights are given by the limiting values, i.e., $k_{ij}=\pm1$. Owing to the symmetry of the system, there are two states: a symmetric and an asymmetric state, as shown in Fig. 13(b). In the symmetric state, the system has two stable solutions in which the weights take the same limiting value. One is an in-phase solution. The weights take the upper limiting value, $k_{12}^*=k_{21}^*=1$, and the oscillators synchronize with the in-phase relation, $\Delta\phi^*=0$. The other is an antiphase solution, $k_{12}^*=k_{21}^*=-1,\Delta\phi^*=\pi$. In the asymmetric state, the weights take different limiting values as $k_{12}^*=1$, $k_{21}=-1$, $\Delta\phi=-\frac{\pi}{2}$ and $k_{12}^*=-1$, $k_{21}=1$, $\Delta\phi=\frac{\pi}{2}$. With the asymmetric coupling weights, one oscillator chases after the other, keeping a $\pi/2$ phase relation. The stability condition of these states is given by $\mathrm{sgn}\,[-\sin(\Delta\phi^*+\beta)]=\mathrm{sgn}\,(k_{12}^*)$ and $\mathrm{sgn}\,[-\sin(-\Delta\phi^*+\beta)]=\mathrm{sgn}\,(k_{21}^*)$, which guarantees that the weights are clamped on the limiting values. In the other parameter region where these states are unstable, the weights seem to converge to zero, as shown in Fig. 13(b). This induces a chaotic state as discussed in Sec. III C.

From the above analysis, we obtain the phase diagram shown in Fig. 13(a).

## APPENDIX B: LINEAR STABILITY OF THE COHERENT STATE AND THE TWO-CLUSTER STATE

In this appendix, we consider the linear stability of the coherent state against a perturbation to the phase variables, $\phi_i$. In this situation, the coupling weight is assumed to be fixed because the time scale of the coupling weight, $1/\epsilon$, is sufficiently large in the limit $\epsilon\to0$. Given the fixed $k_{ij}$, the dynamics of the system are given by

$$\frac{d\phi_i}{dt}=1-\frac{1}{N}\sum_{j\neq i}^{N}k_{ij}\sin(\phi_i-\phi_j+\alpha).\tag{B1}$$

As mentioned in Sec. III B, in the coherent state the phases are uniformly distributed with a fixed relation and the weights satisfy the condition $k_{ij}=\mathrm{sgn}\,(-\sin(\phi_i-\phi_j+\beta))$. Therefore, we define the fixed relative phases $\phi_{ij}^*$ $(\equiv\phi_i^*-\phi_j^*)$ and the weights $k_{ij}^*$ as

$$\phi_{ij}^*=\frac{2\pi(j-i)}{N},$$
$$k_{ij}^*=\mathrm{sgn}\,[-\sin(\phi_{ij}^*+\beta)]=-\mathrm{sgn}\left[\sin\left(\frac{2\pi}{N}(j-i)+\beta\right)\right].$$

First, we calculate the Jacobian matrix $DF_{ij}$. The diagonal components of the Jacobian matrix are expressed by

$$\begin{aligned}DF_{ii}&=-\frac{1}{N}\sum_{j\neq i}k_{ij}^*\cos(\phi_{ij}^*+\alpha)\\&=\frac{1}{N}\sum_{j\neq i}\mathrm{sgn}\,(\sin x_{j-i})\cos(x_{j-i}+\eta),\end{aligned}$$

where $x_m=\frac{2\pi}{N}m+\beta$ and $\eta=\alpha-\beta$. In the limit $N\to\infty$,

$$DF_{ii}=\frac{1}{2\pi}\int_0^{2\pi}\mathrm{sgn}\,(\sin x)\cos(x+\eta)dx=-\frac{2}{\pi}\sin\eta.$$

The off-diagonal components are also expressed by

$$DF_{ij}=\frac{1}{N}k_{ij}^*\cos(\phi_{ij}^*\alpha)=-\frac{1}{N}\mathrm{sgn}\,(\sin x_{j-i})\cos(x_{j-i}+\eta).$$

Let us denote

$$Y_m=-\frac{1}{N}\mathrm{sgn}\,(\sin x_m)\cos(x_m+\eta)\quad(m=1,2,3,\ldots).$$

$Y_m$ is $N$-periodic so that $Y_{m\pm N} = Y_m$. Then, the Jacobian matrix $DF$ is written as

$$\begin{pmatrix} Y_0 & Y_1 & Y_2 & \cdots & Y_{N-1} \\ Y_{N-1} & Y_0 & Y_1 & \cdots & Y_{N-2} \\ \vdots & & \cdots & & \vdots \\ Y_1 & Y_2 & \cdots & & Y_0 \end{pmatrix},$$

where $Y_0 = -\frac{2}{\pi}\sin\eta$. Since $DF$ is a cyclic matrix, the eigenvalues $\lambda_k$ are

$$\lambda_k = Y_0 + \zeta^k Y_1 + \zeta^{2k} Y_2 + \cdots + \zeta^{(N-1)k} Y_{N-1} \quad (k = 0,1,2,\ldots,N-1),$$

and the eigenvectors $v_k$ are

$$v_k = \frac{1}{\sqrt{N}}(1,\zeta^k,\zeta^{2k},\zeta^{3k},\ldots,\zeta^{(N-1)k})^\dagger,$$

where $\zeta$ $(=e^{2\pi i/N})$ is a primitive $N$th root of unity.

Then,

$$\mathrm{Re}\lambda_k = -\frac{2}{\pi}\sin\eta + \sum_{m=1}^{N-1}\cos\left(\frac{2\pi}{N}km\right)\left(-\frac{1}{N}\right) \times \mathrm{sgn}(\sin x_m)\cos(x_m+\eta).$$

Using $\cos(\frac{2\pi}{N}km) = \cos(kx_m - k\beta)$, the equation can be rewritten as

$$\begin{aligned}\mathrm{Re}\lambda_k &= -\frac{2}{\pi}\sin\eta - \frac{1}{N}\sum_{m=1}^{N-1}\cos(kx_m - k\beta)\mathrm{sgn}(\sin x_m)\cos(x_m+\eta) \\ &= -\frac{2}{\pi}\sin\eta - \frac{1}{2\pi}\int_0^{2\pi}\cos(kx - k\beta)\mathrm{sgn}(\sin x)\cos(x+\eta)dx \\ &= \begin{cases} -\frac{2}{\pi}\sin\eta - \frac{2}{\pi(k^2-1)}(\cos k\beta\sin\eta + k\sin k\beta\cos\eta) & (k \text{ is even}), \\ -\frac{2}{\pi}\sin\eta & (k \text{ is odd}). \end{cases}\end{aligned}$$

The first eigenvalue $\lambda_0$ $(=0)$ corresponds to a uniform shift of the phases. Thus, the stability of the coherent state is determined by

$$\max_{k\geqslant 1}\mathrm{Re}\lambda_k < 0. \tag{B2}$$

Next, we consider the linear stability of the two-cluster state. In the two-cluster state, if the oscillators $i,j$ belong to the same cluster, the relative phases and the coupling weights are given by

$$\phi^*_{ij} = 0, \quad k^*_{ij} = 1.$$

If they belong to different clusters, then

$$\phi^*_{ij} = \pi, \quad k^*_{ij} = -1.$$

For this fixed state, the Jacobian matrix $DF$ is given by

$$DF_{ij} = \begin{cases} \frac{-N+1}{N}\cos\alpha & (i=j), \\ \frac{1}{N}\cos\alpha & (i\neq j), \end{cases}$$

which is independent of the ratio of the population size between the two clusters. Then, we obtain the eigenvalue $\lambda_k$ as

$$\lambda_k = \begin{cases} 0 & (k=0), \\ -\cos\alpha & (k\neq 0). \end{cases} \tag{B3}$$

Given that $\alpha \in [0,\pi/2)$, the two-cluster state is always stable against a perturbation of the phases.


[1] S. H. Strogatz, Nature (London) **410**, 268 (2001).
[2] R. Albert and A.-L. Barabási, Rev. Mod. Phys. **74**, 47 (2002).
[3] M. E. J. Newman, SIAM Rev. **45**, 167 (2003).
[4] G. Q. Bi and M. M. Poo, J. Neurosci. **18**, 10464 (1998).
[5] H. Markram, J. Lübke, M. Frotscher, and B. Sakmann, Science **275**, 213 (1997).
[6] N. Caporale and Y. Dan, Ann. Rev. Neurosci. **31**, 25 (2008).
[7] C. Furusawa and K. Kaneko, Phys. Rev. Lett. **90**, 088102 (2003).
[8] S. Jain and S. Krishna, Proc. Natl. Acad. Sci. USA **98**, 543 (2001).
[9] A. Tero *et al.*, Science **327**, 439 (2010).
[10] K. D. Harris *et al.*, Nature (London) **424**, 552 (2003).
[11] T. Gross and B. Blasius, J. R. Soc. Interf. **5**, 259 (2008).
[12] T. Aoki and T. Aoyagi, Phys. Rev. Lett. **102**, 034101 (2009).
[13] Y. Kuramoto, *Chemical Oscillations, Waves, and Turbulence* (Springer, New York, 1984).
[14] J. A. Acebron *et al.*, Rev. Mod. Phys. **77**, 137 (2005).
[15] S. H. Strogatz, Physica D **143**, 1 (2000).
[16] E. M. Izhikevich, Phys. Rev. E **58**, 905 (1998).
[17] D. O. Hebb, *The Organization of Behavior* (Wiley, New York, 1949).
[18] R. K. Niyogi and L. Q. English, Phys. Rev. E **80**, 066213 (2009).
[19] P. Holme and M. E. J. Newman, Phys. Rev. E **74**, 056108 (2006).
[20] F. Vazquez, V. M. Eguiluz, and M. S. Miguel, Phys. Rev. Lett. **100**, 108702 (2008).
[21] D. Tanaka, Phys. Rev. Lett. **99**, 134103 (2007).
[22] D. J. Watts and S. H. Strogatz, Nature (London) **393**, 440 (1998).
[23] A.-L. Barabasi and R. Albert, Science **286**, 509 (1999).

[24] M. Girvan and M. E. J. Newman, Proc. Natl. Acad. Sci. USA **99**, 7821 (2002).
[25] A. Arenas, A. Díaz-Guilera, J. Kurths, Y. Moreno, and C. Zhou, Phys. Rep. **469**, 93 (2008).
[26] T. Ichinomiya, Phys. Rev. E **70**, 026116 (2004).
[27] T.-W. Ko and G. B. Ermentrout, Phys. Rev. E **78**, 016203 (2008).
[28] J. G. Restrepo, E. Ott, and B. R. Hunt, Phys. Rev. E **71**, 036151 (2005).
[29] J. G. Restrepo, E. Ott, and B. R. Hunt, Chaos **16**, 015107 (2006).
[30] H. Kori and A. S. Mikhailov, Phys. Rev. Lett. **93**, 254101 (2004).
[31] J. Gómez-Gardeñes, S. Gómez, A. Arenas, and Y. Moreno, Phys. Rev. Lett. **106**, 128701 (2011).
[32] J. Gómez-Gardeñes, Y. Moreno, and A. Arenas, Phys. Rev. Lett. **98**, 034101 (2007).
[33] H. Nakao and A. S. Mikhailov, Phys. Rev. E **79**, 036214 (2009).
[34] R. Pastor-Satorras and A. Vespignani, Phys. Rev. Lett. **86**, 3200 (2001).
[35] A. Pikovsky, M. Rosenblum, and J. Kurths, *Synchronization* (Cambridge University Press, Cambridge, England, 2001).
[36] K. Okuda, Physica D **63**, 424 (1993).
[37] D. Golomb, D. Hansel, B. Shraiman, and H. Sompolinsky, Phys. Rev. A **45**, 3516 (1992).
[38] P. Tass, Phys. Rev. E **56**, 2043 (1997).
[39] V. Hakim and W.-J. Rappel, Phys. Rev. A **46**, R7347 (1992).
[40] N. Nakagawa and Y. Kuramoto, Prog. Theor. Phys. **89**, 313 (1993).
[41] M. Falcke and H. Engel, Phys. Rev. E **50**, 1353 (1994).
[42] M. Falcke and H. Engel, J. Chem. Phys. **101**, 6255 (1994).
[43] J. Karbowski and G. B. Ermentrout, Phys. Rev. E **65**, 031902 (2002).
[44] P. Seliger, S. C. Young, and L. S. Tsimring, Phys. Rev. E **65**, 041906 (2002).
[45] D. H. Zanette and A. S. Mikhailov, Europhys. Lett. **65**, 465 (2004).
[46] N. Masuda and H. Kori, J. Comput. Neurosci. **22**, 327 (2007).
[47] Y. L. Maistrenko, B. Lysyansky, C. Hauptmann, O. Burylko, and P. A. Tass, Phys. Rev. E **75**, 066207 (2007).
[48] H. Cateau, K. Kitano, and T. Fukai, Phys. Rev. E **77**, 051909 (2008).
[49] M. Chen, Y. Shang, Y. Zou, and J. Kurths, Phys. Rev. E **77**, 027101 (2008).
[50] M. Iwasa, K. Iida, and D. Tanaka, Phys. Rev. E **81**, 046220 (2010).
[51] M. Iwasa and D. Tanaka, Phys. Rev. E **81**, 066214 (2010).
[52] M. Gilson *et al.*, Biol. Cybern. **101**, 411 (2009).
[53] J. M. Pacheco, A. Traulsen, and M. A. Nowak, Phys. Rev. Lett. **97**, 258103 (2006).
[54] M. G. Zimmermann, V. M. Eguíluz, and M. San Miguel, Phys. Rev. E **69**, 065102 (2004).
[55] A. Szolnoki and M. Perc, Europhys. Lett. **86**, 30007 (2009).
[56] A. Szolnoki and M. Perc, New J. Phys. **11**, 093033 (2009).
[57] J. Poncela, J. Gómez-Gardeñes, A. Traulsen, and Y. Moreno, New J. Phys. **11**, 083031 (2009).
[58] M. Perc and A. Szolnoki, Biosystems **99**, 109 (2010).
[59] M. Jiang and P. Ma, Chaos **19**, 013115 (2009).
[60] C. Zhou and J. Kurths, Phys. Rev. Lett. **96**, 164102 (2006).
[61] F. Sorrentino and E. Ott, Phys. Rev. Lett. **100**, 114101 (2008).
[62] V. Volman and M. Perc, New J. Phys. **12**, 043013 (2010).
[63] A. Mondal, S. Sinha, and J. Kurths, Phys. Rev. E **78**, 066209 (2008).